PAPER • OPEN ACCESS

Dynamical attractors in contracting spacetimes dominated by kinetically coupled scalar fields

To cite this article: Anna Ijjas *et al* JCAP12(2021)030

View the article online for updates and enhancements.

Dynamical attractors in contracting spacetimes dominated by kinetically coupled scalar fields

Anna Ijjas,[a,b,1] **Frans Pretorius,**[c] **Paul J. Steinhardt**[c] **and David Garfinkle**[d]

[a]Max Planck Institute for Gravitational Physics,
Hanover, 30167, Germany

[b]Institute for Theory and Computation, Harvard University,
Cambridge, MA, 02138, U.S.A.

[c]Department of Physics, Princeton University,
Princeton, NJ, 08544, U.S.A.

[d]Department of Physics, Oakland University,
Rochester, MI 48309, U.S.A.

E-mail: anna.ijjas@aei.mpg.de, fpretori@princeton.edu, steinh@princeton.edu, garfinkl@oakland.edu

Abstract. We present non-perturbative numerical relativity simulations of slowly contracting spacetimes in which the scalar field driving slow contraction is coupled to a second scalar field through an exponential non-linear σ model-type kinetic interaction. These models are important because they can generate a nearly scale-invariant spectrum of super-Hubble density fluctuations fully consistent with cosmic microwave background observations. We show that the non-linear evolution rapidly approaches a homogeneous, isotropic and flat Friedmann-Robertson-Walker (FRW) geometry for a wide range of inhomogeneous and anisotropic initial conditions. Ultimately, we find, the kinetic coupling causes the evolution to deflect away from flat FRW and towards a novel Kasner-like stationary point, but in general this occurs on time scales that are too long to be observationally relevant.

---

[1]Corresponding author.

Contents

1 Introduction

Cosmic microwave background observations have shown that the spectrum of temperature anisotropies is nearly scale invariant and gaussian with an average amplitude of one part in hundred thousand and no detectable B-mode polarization thus far. According to our current understanding, the temperature anisotropies are an imprint of primordial curvature fluctuations sourced by quantum excitations of one or more scalar fields, the energy density of which dominated the early-universe [2, 14].

In order for the curvature fluctuations to match the observed spectrum, by the time the modes are generated, the cosmological background must be smooth and flat as described by a Friedmann-Robertson-Walker (FRW) geometry with line element $\mathrm{d}s^2 = -\mathrm{d}\tau^2 + a(\tau)^2\mathrm{d}x^i\mathrm{d}x_i$, where $a(\tau)$ is the FRW scale factor. Then, once the modes are generated, the smoothing mechanism must continue for at least 60 additional e-folds. Neither of these two conditions is trivial to satisfy. For example, if the FRW solution is a robust attractor for a wide range of initial conditions, most of the volume is eventually smoothed and flattened by the time the smoothing phase ends; but, if the smoothing is *not sufficiently rapid*, most volume converges to a smooth and flat FRW spacetime with only a few e-foldings remaining before the end of smoothing. In this case, modes generated around the 60 e-fold mark would carry an imprint of an unsmoothed inhomogeneous and/or anisotropic geometry and would thus not match the observed spectrum.

Slow contraction [3], a primordial phase that connects to the hot expanding phase through a gentle classical bounce, has been shown to be both robust and rapid. The phase can be reached via a canonical scalar field ϕ that is minimally coupled to Einstein gravity and

has a negative potential $V(\phi)$. The scalar field energy density naturally evolves to dominate the total stress-energy while driving the geometry to a smooth and flat FRW space-time. The robustness of slow contraction as a dynamical attractor — its insensitivity to initial conditions including those that lie outside the perturbative regime of FRW spacetimes — was recently shown in refs. [6, 9, 11]; the remarkable rapidity, with smoothing and flattening typically occurring within less than 10 e-folds of contraction of the Hubble radius, was demonstrated in ref. [9].

The goal of this paper is to examine whether the powerful smoothing property remains in cases in which the smoothing scalar field ϕ is coupled to a second scalar field χ through an exponential non-linear σ model-type kinetic interaction. These models are important because it has been shown that they can lead to the generation of a nearly scale-invariant spectrum of super-Hubble density fluctuations fully consistent with cosmic microwave background observations [12, 13]. More generally, this study is important for exploring whether slow contraction remains a powerful, robust and rapid dynamical attractor even when there is an exponentially strong kinetic interaction with a secondary scalar field and whether any distinctive features result compared to the case of scalar fields with canonical kinetic energy density.

As demonstrated in ref. [11], the key to rapid and robust smoothing is *ultralocality*: starting with arbitrary initial data that lies outside the perturbative regime of the FRW state, contracting spacetimes rapidly evolve to an anisotropic and spatially curved state where gradients, i.e., spatial derivatives, are suppressed relative to the other so-called *velocity* contributions. These causally separated regions then each independently evolve to the homogeneous, isotropic and spatially flat FRW state which is the only stable stationary point of the ultralocal limit.

Once the flat FRW state is reached, physical distances between objects shrink proportional to the scale factor $a(\tau)$ and exponentially slower than the Hubble radius,

$$|H^{-1}| \equiv |\mathrm{d}\ln a(\tau)/\mathrm{d}\tau|^{-1} \propto a^{\epsilon_\phi}, \tag{1.1}$$

where $\epsilon_\phi \gg 3$; hence the name: slow contraction. The rate at which $|H^{-1}|$ contracts is determined by the effective equation of state associated with the scalar field on an FRW background:

$$\epsilon_\phi \equiv \frac{3}{2}\left(1 + \frac{p_\phi}{\rho_\phi}\right) = 3 \times \frac{\frac{1}{2}\phi'^2}{\frac{1}{2}\phi'^2 + V(\phi)}, \tag{1.2}$$

where $p_\phi = \frac{1}{2}\phi'^2 - V(\phi)$ is the co-moving 'pressure' and $\rho_\phi = \frac{1}{2}\phi'^2 + V(\phi)$ the co-moving energy density of the scalar field ϕ in the homogeneous FRW limit and prime denotes differentiation with respect to τ.

For a negative exponential potential,

$$V(\phi) = -V_0 e^{-\phi/M}, \quad V_0 > 0, \tag{1.3}$$

as will be considered throughout this paper, the scaling attractor solution of the Einstein-scalar system in the flat FRW limit is given by

$$a(\tau) = (-\tau)^{1/\epsilon_\phi}, \quad \phi(\tau) = M_{\mathrm{Pl}}\sqrt{\frac{2}{\epsilon_\phi}} \times \ln(-A\,\tau), \quad \epsilon_\phi = \frac{1}{2} \times \left(\frac{M_{\mathrm{Pl}}}{M}\right)^2, \tag{1.4}$$

where $A = M_{\mathrm{Pl}}^{-1}\epsilon_\phi\sqrt{V_0/(\epsilon_\phi - 3)}$ and τ is running from large negative to small negative values. (Here and throughout the paper, reduced Planck units, $M_{\mathrm{Pl}}^{-2} \equiv 8\pi G_{\mathrm{N}}$ with G_{N} being

Newton's constant, are used.) For a potential with the characteristic mass scale $M \sim 0.1\,M_{\rm Pl}$, the effective equation of state $\epsilon_\phi = 50$ is such that the scale factor contracts only by a factor of 2 while the Hubble radius shrinks by a factor of 2^{50}.

A particularly important feature of slow contraction is the fact that, because the Hubble radius shrinks much faster than the scale factor, the wavelengths of fluctuations (which are proportional to $a(\tau)$) necessarily end up on super-Hubble scales by the end of slow contraction. Unlike inflation, though, slow contraction is a 'supersmoother,' meaning that adiabatic (*a.k.a.* curvature) modes decay, whether they are of classical or quantum origin [4]. The decay is the opposite of what occurs in expanding universes and is associated with the fact that the evolution of the adiabatic modes during slow contraction is subject to an antifriction-like term ($H \ll 0$) that has the opposite sign than the friction-like term ($H \gg 0$) in the expanding case. This is an important and appealing feature of slow contraction because it suppresses quantum runaway effects. At the same time, a mechanism is needed to generate the spectrum of temperature anisotropies observed in the cosmic microwave background and the seeds for structure formation.

In refs. [12, 13], it has been shown that entropy modes (i.e. pressure fluctuations on hypersurfaces of constant energy density) generated by quantum fluctuations of a second scalar field during slow contraction can fulfill this role. First, like adiabatic modes, the entropic modes are generated by quantum fluctuations and their wavelengths also end up on super-Hubble scales. Second, unlike the adiabatic modes, the entropy modes can experience a net red shift effect. This can occur, for example, if the modes are sourced by a light scalar field χ that is kinetically coupled to the background field ϕ through a non-linear σ-type interaction, e.g.,

$$\mathcal{S} = \int {\rm d}^4x \sqrt{-g}\Big(\tfrac{1}{2}M_{\rm Pl}{}^2 R - \tfrac{1}{2}\nabla_\mu\phi\nabla^\mu\phi - V(\phi) - \tfrac{1}{2}\kappa(\phi)\nabla_\mu\chi\nabla^\mu\chi - U(\chi)\Big), \qquad (1.5)$$

where g is the four-metric determinant and R the Ricci scalar.

Assuming an exponential coupling

$$\kappa(\phi) = e^{-\phi/m} \qquad (1.6)$$

with a characteristic mass scale $m \lesssim M$ as will be considered throughout this paper, the stable attractor solution of the Friedmann-scalar system of equations with $U(\chi) \simeq 0$,

$$3M_{\rm Pl}^2 H^2 = \frac{1}{2}\phi'^2 + \frac{1}{2}\kappa(\phi)\chi'^2 - V_0 e^{-\phi/M}, \qquad (1.7)$$

$$\phi'' + 3H\phi' + \frac{V_0}{M}e^{-\phi/M} = \frac{1}{2}\kappa_{,\phi}\chi'^2, \qquad (1.8)$$

$$\chi'' + \left(3H + \frac{\kappa_{,\phi}}{\kappa}\phi'\right)\chi' = 0, \qquad (1.9)$$

is that χ is constant ($\chi' \equiv 0$) while $a(\tau)$ and $\phi(\tau)$ evolve with time according to the scaling solution given by eq. (1.4). The constant χ solution is stable [12] because, on an FRW background, the kinetic coupling $\frac{1}{2}\kappa(\phi)\nabla_\mu\chi\nabla^\mu\chi$ enters the evolution equation (2.25) of the χ-field in a way that adds to the Hubble anti-friction a friction-like term,

$$3H \rightarrow 3H + \frac{\kappa_{,\phi}}{\kappa}\phi' = \frac{1}{\epsilon_\phi(-\tau)}\left(\frac{M_{\rm Pl}^2}{m \times M} - 3\right) \gg 0. \qquad (1.10)$$

Since the combination is positive, the χ field's kinetic energy experiences a net damping as if it were in a de Sitter-like background and freezes out at some constant value. Notably, quantum fluctuations of the χ field also experience a net de Sitter-like damping term $3H + \phi'/m \gg 0$ such that their amplitude grows, leading to a nearly scale-invariant and gaussian spectrum of entropy modes on super-Hubble wavelengths. Finally, it has been shown that the entropy modes can source curvature modes, e.g. when exiting slow contraction and entering the bounce stage, as shown in refs. [7, 8].

The remaining question is whether adding a χ field with the exponential non-linear σ model-type kinetic interaction with ϕ needed to generate a nearly scale-invariant and gaussian spectrum of curvature perturbations preserves the robustness and rapidity of slow contraction as established for the single field scenario. In this paper, we address this issue by adapting the mathematical and numerical techniques developed for the single-field case in refs. [3, 5, 6, 9, 11].

Our non-perturbative analysis yields some surprising results that could not be obtained using the conventional methods of cosmological perturbation theory. First, in the special case where χ is precisely massless, we find that the evolution can be rapidly deflected away from the flat FRW stationary point if the characteristic scale M associated with $V(\phi)$ is too close to the Planck scale ($M = 1$), or equivalently, if ε_ϕ is not sufficiently large; instead, the evolution is driven towards a Kasner-like solution in which the gradient of χ, $\bar{S}_\chi{}^x(\tau, x)$, is non-zero and time-independent

$$\partial_\tau \bar{S}_\chi{}^x \equiv 0. \tag{1.11}$$

Second, in generic models which have moderately smaller values of $M \lesssim 0.1$ or weakly broken shift symmetry in χ, e.g., a small mass for χ, we find that the deflection effect is strongly suppressed such that the evolution leads to a long-lived state with negligible $S_\chi{}^x(\tau, x)$ and the FRW scaling solution in eq. (1.4), similar to the impressive single-field result. This state persists long enough and has just the conditions needed to generate a nearly scale-invariant spectrum of curvature perturbations that can account for temperature fluctuations observed in the cosmic microwave background. The kinetic coupling ultimately causes the evolution to deflect from flat FRW, but on a time scale that is too long to be relevant for cosmologies that connect to the hot expanding phase through a smooth (non-singular) bounce.

2 Numerical scheme

For the non-perturbative, numerical analysis, we shall adapt the orthonormal tetrad form of the Einstein-scalar field equations corresponding to the action given in eq. (1.5),

$$G_{\mu\nu} = \nabla_\mu\phi\nabla_\nu\phi + \kappa(\phi)\nabla_\mu\chi\nabla_\nu\chi \tag{2.1}$$
$$- \left(\tfrac{1}{2}\nabla_\sigma\phi\nabla^\sigma\phi + \tfrac{1}{2}\kappa(\phi)\nabla_\sigma\chi\nabla^\sigma\chi + V(\phi) + U(\chi)\right)g_{\mu\nu},$$
$$\Box\phi = V_{,\phi} + \tfrac{1}{2}\kappa_{,\phi}\nabla_\sigma\chi\nabla^\sigma\chi, \tag{2.2}$$
$$\Box\chi = U_{,\chi} - \frac{\kappa_{,\phi}}{\kappa}\nabla^\sigma\phi\nabla_\sigma\chi, \tag{2.3}$$

as developed for the single-field case. As per convention, $g_{\mu\nu}$ is the spacetime metric, and $G_{\mu\nu}$ is the Einstein tensor. (Here and for the remainder of the paper, we express dimensional quantities in reduced Planck units where $M_{\rm Pl} = 1$.) Throughout, spacetime indices $(0-3)$ are Greek and spatial indices $(1-3)$ are Latin. The beginning of the alphabet $(\alpha, \beta, \gamma$ or $a, b, c)$ denotes tetrad indices and the middle of the alphabet $(\mu, \nu, \rho$ or $i, j, k)$ denotes coordinate

indices. In the following, we only give a brief overview with the goal of making the paper self-contained. A comprehensive description of the formulation as well as a complete derivation of the evolution and constraint equations are provided in refs. [6, 11].

2.1 Variables

As with any tetrad formulation of the field equations, spacetime points are represented through a family of unit basis four-vectors, or *vierbein*, $\{e_0, e_1, e_2, e_3\}$, where e_0 is the timelike four-vector and the spacelike four-vectors of the triad $\{e_1, e_2, e_3\}$ each lie in the rest three-space of e_0. The local Lorentz frame set by the tetrad basis is flat, i.e.,

$$g_{\alpha\beta} = e_\alpha \cdot e_\beta = \eta_{\alpha\beta}, \tag{2.4}$$

with $\cdot$ denoting the inner product of the tetrad and $\eta_{\alpha\beta} = \mathrm{diag}(-1, 1, 1, 1)$ being the Minkowski metric.

The *geometric variables* of the formulation are the sixteen tetrad vector components $\{e_\alpha{}^\mu\}$ and the twenty-four Ricci rotation coefficients

$$\gamma_{\alpha\beta\lambda} \equiv e_\alpha \nabla_\lambda e_\beta, \tag{2.5}$$

where ∇_λ is the projection of the spacetime covariant derivative ∇_μ onto the tetrad e_λ, $\nabla_\lambda \equiv e_\lambda{}^\mu \nabla_\mu$;

$$K_{ab} \equiv -\gamma_{0ba} \tag{2.6}$$

defines the nine components of the shear tensor; and

$$N_{ab} \equiv \tfrac{1}{2}\epsilon_b{}^{cd}\gamma_{cda}, \tag{2.7}$$

is the induced curvature tensor associated with the spatial triad where ϵ_{abc} denotes the Levi-Civita-symbol. The eighteen components of K_{ab} and N_{ab} are *dynamical* variables. The three-vectors

$$b_a \equiv \gamma_{a00}, \quad \Omega_a \equiv \frac{1}{2}\epsilon_a{}^{bc}\gamma_{cb0} \tag{2.8}$$

are frame *gauge* quantities with b_a defining the proper local acceleration of the congruence and Ω_a defining the local angular velocity of the spatial triad relative to Fermi-propagated axes.

The geometric variables must be supplemented by the variables describing the two scalars. These are the field distributions ϕ, χ, their velocities and gradients, respectively, as detailed below in section 2.3.

2.2 Gauge fixing

For our numerical scheme, we fix the six gauge degrees of freedom of the *tetrad frame* in a way that makes the connection of the geometric variables to physical quantities straightforward:

- we fix the spatial triad $\{e_1, e_2, e_3\}$ to be inertially non-rotating a.k.a. *Fermi propagated* ($\Omega_a \equiv 0$);

- we require the shear tensor to be symmetric ($K_{ab} \equiv K_{(ab)}$), meaning that the tetrad congruence is *hypersurface-orthogonal* such that it defines a particular foliation of spacetime into spacelike hypersurfaces of constant time $\{\Sigma_t\}$ with e_0 being the future directed timelike unit normal to $\{\Sigma_t\}$ and the spatial triad vectors being tangent to $\{\Sigma_t\}$.

With this choice of tetrad frame gauge, K_{ab} denotes the extrinsic curvature of $\{\Sigma_t\}$ and the components of N_{ab} are the spatial (or intrinsic) curvature variables. Note that the acceleration vector b_a is implicitly fixed by this gauge choice through

$$b_a \times e_0(x^0) = -e_a e_0(x^0), \tag{2.9}$$

where x^0 is the time coordinate of $\{\Sigma_t\}$ and $\times$ denotes scalar multiplication.

Furthermore, we must write the tetrad evolution and constraint equations in the form of partial differential equations (PDEs) by way of which we shall numerically evolve the geometric and scalar field variables specified on an initial spacelike hypersurface. To do so is particularly straightforward given our choice of a hypersurface-orthogonal tetrad because, in this frame gauge, elements of the transformation matrix $\{\lambda_\alpha{}^\mu\}$ between tetrad and coordinate basis four-vectors,

$$e_\alpha = \lambda_\alpha{}^\mu e_\mu, \tag{2.10}$$

are easily identified with quantities of the 3+1 Arnowitt-Deser-Misner (ADM) formalism, namely:

$$\lambda_0{}^0 = N^{-1}, \quad \lambda_0{}^i = -N^i/N, \quad \lambda_a{}^0 = 0, \quad \lambda_a{}^i = E_a{}^i, \tag{2.11}$$

where N is the ADM lapse, N^i the ADM shift and the coordinate metric is being given by $g^{\mu\nu} = \eta^{\alpha\beta} \lambda_\alpha{}^\mu \lambda_\beta{}^\nu$. Finally, the directional derivatives along the tetrads can be written as

$$D_0 = N^{-1}(\partial_t - N^i \partial_i), \quad D_a = E_a{}^i \partial_i. \tag{2.12}$$

To fix the four *coordinate* gauge degrees of freedom, we specify the lapse function N and the shift vector N^i by requiring that

- surfaces of constant time $\{\Sigma_t\}$ have constant mean curvature (CMC), i.e., $\Theta^{-1} \equiv -\frac{1}{3} K_a{}^a = const.$ The CMC slicing condition fixes the lapse function in that it leads to an elliptic equation (2.17) for N; and

- the spatial coordinates are co-moving ($N_i = 0$), i.e. constant along both the congruence and the foliation.

As emphasized previously in refs. [6, 11], the particular choice of our coordinate gauge has several advantages: since the trace of the extrinsic curvature Θ^{-1} is spatially uniform on each $\{\Sigma_t\}$, we can define the time coordinate t to track Θ, i.e.,

$$e^t = \tfrac{1}{3}\Theta, \tag{2.13}$$

such that, in the homogeneous limit, Θ is the Hubble radius $|H^{-1}|$. In addition, we can use Θ to rewrite our equations in terms of dimensionless Hubble-normalized variables,

$$N \to \mathcal{N} \equiv N/\Theta, \tag{2.14}$$

$$\{K_{ab}, N_{ab}, E_a{}^i\} \to \{\bar{K}_{ab}, \bar{N}_{ab}, \bar{E}_a{}^i\} \equiv \{K_{ab}, N_{ab}, E_a{}^i\} \times \Theta, \tag{2.15}$$

$$\{V, U\} \to \{\bar{V}, \bar{U}\} \equiv \{V, U\} \times \Theta^2, \tag{2.16}$$

where $\mathcal{N}$ is the Hubble-normalized lapse and bar denotes normalization by the mean curvature Θ^{-1} on constant time hypersurfaces.

The combination of the time coordinate t tracking the three-curvature with Hubble-normalized variables is particularly useful for our purposes to study the rapidity and robustness

– 6 –

of slow contraction because it enables us to run the simulation for any finite period without encountering singular behavior or stiffness issues: first, the putative singularity is at $t \to -\infty$ and, second, the rapidly changing Hubble radius is not entering the numerical calculation as a dynamical variable, leaving the slowly changing scale factor as the only relevant dynamical factor.

2.3 Evolution and constraint equations

Taking everything together, the Einstein-scalar field evolution equations (2.1)–(2.3) in Hubble-normalized, orthonormal tetrad form yield an elliptic-hyperbolic system: the lapse $\mathcal{N}$ is defined at each time step through an elliptic equation,

$$- D^a D_a \mathcal{N} + 2\bar{A}^b D_b \mathcal{N} + \mathcal{N}\left(3 + \bar{\Sigma}_{ab}\bar{\Sigma}^{ab} + \bar{W}_\phi^2 + \bar{W}_\chi^2 - \bar{V}(\phi) - \bar{U}(\chi)\right) = 3\,; \qquad (2.17)$$

while the evolution of the remaining geometric as well as the scalar field variables is given by a hyperbolic system of PDEs:

$$\partial_t \bar{E}_a{}^i = \bar{E}_a{}^i - \mathcal{N}\left(\bar{E}_a{}^i + \bar{\Sigma}_a{}^b \bar{E}_b{}^i\right), \qquad (2.18)$$

$$\partial_t \bar{A}_b = \bar{A}_b + \tfrac{1}{2}\bar{\Sigma}_b{}^c D_c \mathcal{N} - D_b \mathcal{N} + \mathcal{N}\left(\tfrac{1}{2}D_c\bar{\Sigma}_b{}^c - \bar{A}_b - \bar{\Sigma}_b{}^c \bar{A}_c\right), \qquad (2.19)$$

$$\partial_t \bar{n}^{ab} = \bar{n}^{ab} - \epsilon^{cd(a}\bar{\Sigma}_d{}^{b)}D_c\mathcal{N} + \mathcal{N}\left(-\bar{n}^{ab} + 2\bar{n}^{(a}{}_c\bar{\Sigma}^{b)c} - \epsilon^{cd(a}D_c\bar{\Sigma}_d{}^{b)}\right), \qquad (2.20)$$

$$\partial_t \bar{\Sigma}_{ab} = \bar{\Sigma}_{ab} + D_{\langle a}D_{b\rangle}\mathcal{N} + \bar{A}_{\langle a}D_{b\rangle}\mathcal{N} + \epsilon_{cd(a}\bar{n}_{b)}{}^d D^c\mathcal{N} \qquad (2.21)$$
$$\quad - \mathcal{N}\left(3\bar{\Sigma}_{ab} + D_{\langle a}\bar{A}_{b\rangle} + 2\bar{n}_{\langle a}{}^c \bar{n}_{b\rangle c} - \bar{n}_c{}^c \bar{n}_{\langle ab\rangle} - \epsilon_{cd(a}\left(D^c\bar{n}_{b)}{}^d - 2\bar{A}^c\bar{n}_{b)}{}^d\right)\right)$$
$$\quad + \mathcal{N}\left(\bar{S}_{\phi\langle a}\bar{S}_{\phi b\rangle} + \bar{S}_{\chi\langle a}\bar{S}_{\chi b\rangle}\right),$$

$$\partial_t \phi = \mathcal{N}\bar{W}_\phi, \qquad (2.22)$$

$$\partial_t \bar{S}_{\phi a} = \bar{S}_{\phi a} + \bar{W}_\phi D_a \mathcal{N} + \mathcal{N}\left(D_a\bar{W}_\phi - \left(\bar{S}_{\phi a} + \bar{\Sigma}_a{}^b \bar{S}_{\phi b}\right)\right), \qquad (2.23)$$

$$\partial_t \bar{W}_\phi = \bar{W}_\phi + \bar{S}_\phi{}^a D_a \mathcal{N} + \mathcal{N}\left(D^a\bar{S}_{\phi a} - 3\bar{W}_\phi - 2\bar{A}^b\bar{S}_{\phi b} - \bar{V}_{,\phi}\right) \qquad (2.24)$$
$$\quad + \tfrac{1}{2}\mathcal{N}\frac{\kappa_{,\phi}}{\kappa}\left(\bar{W}_\chi^2 - \bar{S}_\chi{}^a\bar{S}_{\chi a}\right),$$

$$\partial_t \chi = \mathcal{N}\frac{\bar{W}_\chi}{\sqrt{\kappa(\phi)}}, \qquad (2.25)$$

$$\partial_t \bar{S}_{\chi a} = \bar{S}_{\chi a} + \bar{W}_\chi D_a \mathcal{N} + \mathcal{N}\left(D_a\bar{W}_\chi - \left(\bar{S}_{\chi a} + \bar{\Sigma}_a{}^b \bar{S}_{\chi b}\right)\right) \qquad (2.26)$$
$$\quad + \tfrac{1}{2}\frac{\kappa_{,\phi}}{\kappa}\mathcal{N}\left(\bar{W}_\phi\bar{S}_{\chi a} - \bar{W}_\chi\bar{S}_{\phi a}\right),$$

$$\partial_t \bar{W}_\chi = \bar{W}_\chi + \bar{S}_\chi{}^a D_a \mathcal{N} + \mathcal{N}\left(D^a\bar{S}_{\chi a} - 3\bar{W}_\chi - 2\bar{A}^b\bar{S}_{\chi b} - \frac{\bar{U}_{,\chi}}{\sqrt{\kappa}}\right) \qquad (2.27)$$
$$\quad + \tfrac{1}{2}\mathcal{N}\frac{\kappa_{,\phi}}{\kappa}\left(\bar{S}_\phi{}^a\bar{S}_{\chi a} - \bar{W}_\phi\bar{W}_\chi\right),$$

where curved brackets denote symmetrization $X_{(ab)} \equiv \frac{1}{2}(X_{ab} + X_{ba})$ and angle brackets denote traceless symmetrization defined as $X_{\langle ab\rangle} \equiv X_{(ab)} - \frac{1}{3}X_c{}^c\delta_{ab}$. The geometric variables

$$\bar{n}_{ab} \equiv \bar{N}_{(ab)}, \quad \bar{A}_b \equiv \tfrac{1}{2}\epsilon_b{}^{cd}\bar{N}_{cd}, \qquad (2.28)$$

are the symmetric and antisymmetric components, respectively of the Hubble-normalized, spatial curvature tensor $\bar{N}_{ab}$; $\bar{\Sigma}_{ab}$ is the trace-free extrinsic curvature tensor,

$$\bar{\Sigma}_{ab} \equiv \bar{K}_{ab} - \delta_{ab}. \tag{2.29}$$

The variables

$$\bar{W}_\phi \equiv \mathcal{N}^{-1}\partial_t\phi, \quad \bar{W}_\chi \equiv \mathcal{N}^{-1}\partial_t\chi \tag{2.30}$$

denote the Hubble-normalized scalar field velocities.

In addition, the evolution equations are supplemented by a set of constraints which we shall use to specify the initial data as well as to verify convergence of the numerical computation:

$$\bar{A}^b\bar{A}_b - \tfrac{2}{3}D_b\bar{A}^b + \tfrac{1}{6}\bar{n}^{ab}\bar{n}_{ab} - \tfrac{1}{12}(\bar{n}_a{}^a)^2 + \tfrac{1}{6}\bar{\Sigma}^{ab}\bar{\Sigma}_{ab} \tag{2.31}$$
$$+ \tfrac{1}{6}\left(\bar{W}_\phi^2 + \bar{S}_\phi{}^a\bar{S}_{\phi a}\right) + \tfrac{1}{3}\bar{V}(\phi) + \tfrac{1}{6}\left(\bar{W}_\chi^2 + \bar{S}_\chi{}^a\bar{S}_{\chi a}\right) + \tfrac{1}{3}\bar{U}(\chi) = 1,$$

$$D_b\bar{\Sigma}_a{}^b - 3\bar{\Sigma}_a{}^b\bar{A}_b - \epsilon_{abc}\bar{n}^{bd}\bar{\Sigma}_d{}^c - \bar{W}_\phi\bar{S}_{\phi a} - \bar{W}_\chi\bar{S}_{\chi a} = 0\,, \tag{2.32}$$

$$D_a\bar{n}^{ac} + \epsilon^{abc}D_a\bar{A}_b - 2\bar{A}_a\bar{n}^{ac} = 0\,, \tag{2.33}$$

$$\epsilon^{abk}\left(D_a\bar{E}_b{}^l - \bar{A}_a\bar{E}_b{}^l\right) - \bar{n}^{kc}\bar{E}_c{}^l = 0\,, \tag{2.34}$$

$$\bar{S}_{\phi a} = D_a\phi\,, \tag{2.35}$$

$$\bar{S}_{\chi a} = \sqrt{\kappa(\phi)}\, D_a\chi\,. \tag{2.36}$$

The variables $\bar{S}_{\phi a}, \bar{S}_{\chi a}$ denote the Hubble-normalized scalar field gradients. Note that, for simplicity, we rescaled the velocity and gradient terms of the χ field with the non-linear σ-type kinetic interaction $\kappa(\phi)$, as can be seen, e.g., in eqs. (2.25) and (2.36).

3 Initial data

To study the robustness of the kinetically-coupled two-field model as given through eq. (1.5) to cosmic initial conditions, it is essential to perform a large number of numerical relativity simulations corresponding to a wide range of initial conditions including those that lie far outside the perturbative regime of homogeneous and isotropic FRW spacetimes.

As detailed in refs. [6, 11], our numerical scheme allows for the variation of all freely specifiable geometric and scalar field variables, $\{\bar{E}_a{}^i, \bar{n}_{ab}, \bar{A}_b, \bar{\Sigma}_{ab}\}$ and $\{\phi, \chi, \bar{W}_\phi, \bar{W}_\chi\}$, respectively. To ensure that the initial data satisfy the constraint equations (2.31)–(2.36), in particular, energy and momentum conservation, we adapt, as in our earlier work, the York method [15] that is commonly used in numerical relativity studies. (If the constraint equations are satisfied at the initial time, the Einstein equations propagate them such that they are satisfied at all later times, a condition that is checked numerically.)

Employing the same tetrad frame and coordinate gauge conditions that we detailed above in section 2.2, we first fix the value of the inverse mean curvature Θ_0 of the spatial hypersurface Σ_{t_0} at some initial time t_0 and then define the three-metric of Σ_{t_0} to be *conformally-flat*, i.e.,

$$g_{ij}(t_0, \mathbf{x}) = \psi^4(t_0, \mathbf{x})\delta_{ij}, \tag{3.1}$$

where the conformal factor ψ is not a free function but is determined by an elliptic equation (given in eq. (3.11) below) upon setting all other variables. Note that the conformally-flat

metric choice in eq. (3.1) does not impose a limitation on cases that can be studied since it does not propagate; in fact, it is immediately violated after the first evolution step.

Our choice of Θ_0 and $g_{ij}(t_0, \mathbf{x})$ fixes the coordinate components of the spatial tetrad basis vectors,

$$\bar{E}_a{}^i(t_0, \mathbf{x}) = \psi^{-2}(t_0, \mathbf{x})\Theta_0\delta_a{}^i, \tag{3.2}$$

and the intrinsic curvature variables,

$$\bar{n}_{ab}(t_0, \mathbf{x}) = 0, \quad \bar{A}_b(t_0, \mathbf{x}) = -2\psi^{-1}(t_0, \mathbf{x})\bar{E}_b{}^i(t_0, \mathbf{x})\partial_i\psi(t_0, \mathbf{x}). \tag{3.3}$$

Upon substitution of eqs. (3.2)–(3.3), it is straightforward to verify that the constraints (2.33) and (2.34) are trivially satisfied.

Furthermore, with a conformally-flat spatial metric, the momentum constraint (2.32) reduces to the following simple relation,

$$\partial^b Z_{ab}^0 = Q_\phi\partial_a\phi + Q_\chi\sqrt{\kappa(\phi)}\partial_a\chi, \tag{3.4}$$

where

$$Z_{ab}^0 \equiv \psi^6(t_0, \mathbf{x})\bar{\Sigma}_{ab}(t_0, \mathbf{x}), \tag{3.5}$$

$$Q_\phi(t_0, \mathbf{x}) \equiv \psi^6(t_0, \mathbf{x})\bar{W}_\phi(t_0, \mathbf{x}), \quad Q_\chi(t_0, \mathbf{x}) \equiv \psi^6(t_0, \mathbf{x})\bar{W}_\chi(t_0, \mathbf{x}), \tag{3.6}$$

denote the conformally rescaled Hubble-normalized shear and scalar field velocity variables, respectively.

For simplicity and without loss of generality, we choose the initial value of ϕ and χ to be zero,

$$\phi(t_0, \mathbf{x}) = 0, \quad \chi(t_0, \mathbf{x}) = 0, \tag{3.7}$$

turning the *momentum* constraint (3.4) into the condition that the initial shear component Z_{ab}^0 be divergence free and giving us full freedom to choose the initial scalar field velocities Q_ϕ and Q_χ.

We fix these quantities as follows:

$$Z_{ab}^0 = \begin{pmatrix} b_2 & \xi & 0 \\ \xi & a_1\cos x + b_1 & a_2\cos x \\ 0 & a_2\cos x & -b_1 - b_2 - a_1\cos x \end{pmatrix}, \tag{3.8}$$

and

$$Q_\phi(t_0, \mathbf{x}) = \Theta_0\Big(f_\phi\cos\left(\mu_\phi x + d_\phi\right) + Q_0\Big), \tag{3.9}$$

$$Q_\chi(t_0, \mathbf{x}) = \Theta_0\Big(f_\chi\cos\left(\mu_\chi x + d_\chi\right)\Big), \tag{3.10}$$

where the parameters ξ, a_1, a_2, $b_1, b_2, f_\phi, \mu_\phi, d_\phi, f_\chi, \mu_\chi, d_\chi$, and Q_0 are constants. The sinusoidal form reflects the fact that, for the numerical simulation, we choose periodic boundary conditions $0 \leq x \leq 2\pi$ with 0 and 2π identified. For simplicity, all deviations from homogeneity are along a single spatial direction x, as in ref. [6].

Finally, with the initial value of all freely specifiable geometric and scalar field variables $\Theta_0, \bar{E}_a{}^i, \bar{A}_b, \bar{n}_{ab}, Z_{ab}^0, \phi, \chi, Q_\phi, Q_\chi$ fixed and satisfying the constraint equations (2.32)–(2.36), we impose the remaining *Hamiltonian* constraint (2.31) on these variables. This yields an elliptic equation for the conformal factor ψ,

$$\partial^a\partial_a\psi = \tfrac{1}{4}\Theta_0^{-2}\left(3 - \bar{V} - \bar{U}\right)\psi^5 - \tfrac{1}{8}\left(\partial^a\phi\partial_a\phi\right)\psi - \tfrac{1}{8}\Theta_0^{-2}\left(Q_\phi^2 + Q_\chi^2 + Z^{ab}Z_{ab}\right)\psi^{-7}, \tag{3.11}$$

which we solve numerically.

4 Numerical results

To numerically solve the Einstein-scalar field equations, we discretize the elliptic-hyperbolic system (2.17)–(2.27) using second order accurate spatial derivatives and a three-step method for time integration employing the Iterated Crank-Nicolson algorithm. At each sub-step, we first solve the elliptic equation (2.17) for the Hubble-normalized lapse $\mathcal{N}$ through a relaxation method and then update the hyperbolic equations (2.18)–(2.27) to the next Iterated Crank-Nicolson sub-step. In the simulations presented below, we use a grid of 4096 points with $\Delta x = 2\pi/4096$ and a Courant factor of 0.5. To demonstrate the convergence of our code, the error and convergence was analyzed for a broad range of examples using the same methods as detailed in the appendices of refs. [6, 9]. To summarize those tests, our code shows no signs of numerical instability and exhibits clear second order convergence at early times. At later times when a smooth, ultralocal spacetime develops, we empirically see the convergence improve to third order.

In this section, we present three representative examples from our extensive numerical studies of slow contraction with kinetically coupled scalar fields ϕ and χ given through the action in eq. (1.5) with kinetic coupling

$$\kappa(\phi) = e^{-\phi/m} \tag{4.1}$$

and potential energy densities

$$V(\phi) = -V_0 e^{-\phi/M} \quad \text{and} \quad U(\chi) = \frac{1}{2} m_\chi^2 \chi^2, \tag{4.2}$$

respectively. We begin with the special case that $m_\chi = 0$ and demonstrate a subtle instability compared to the single-field case in refs. [6, 9, 11]. We then show that, for the generic case with $m_\chi \neq 0$, the instability is suppressed and robust and rapid convergence to a long-lived flat FRW state occurs.

For each example, we show the evolution of the total scalar field energy density ($\Omega_{\phi-\chi}$), shear (Ω_s) and curvature (Ω_k) contributions to the normalized energy density, defined as:

$$\Omega_{\phi-\chi} = \tfrac{1}{6}\bar{W}_\phi^2 + \tfrac{1}{6}\bar{S}_\phi{}^a \bar{S}_{\phi a} + \tfrac{1}{3}\bar{V} + \tfrac{1}{6}\bar{W}_\chi^2 + \tfrac{1}{6}\bar{S}_\chi{}^a \bar{S}_{\chi a} + \tfrac{1}{3}\bar{U} \tag{4.3}$$

$$\Omega_s \equiv \tfrac{1}{6}\bar{\Sigma}^{ab}\bar{\Sigma}_{ab} \tag{4.4}$$

$$\Omega_k \equiv -\tfrac{2}{3}D_b\bar{A}^b + \bar{A}^b\bar{A}_b + \tfrac{1}{6}\bar{n}^{ab}\bar{n}_{ab} - \tfrac{1}{12}(\bar{n}_a{}^a)^2, \tag{4.5}$$

where $\Omega_{\phi-\chi} + \Omega_s + \Omega_k = 1$. We also formally define the separate contributions of the two fields,

$$\Omega_\phi \equiv \tfrac{1}{6}\bar{W}_\phi^2 + \tfrac{1}{6}\bar{S}_\phi{}^a \bar{S}_{\phi a} + \tfrac{1}{3}\bar{V}, \tag{4.6}$$

$$\Omega_\chi \equiv \tfrac{1}{6}\bar{W}_\chi^2 + \tfrac{1}{6}\bar{S}_\chi{}^a \bar{S}_{\chi a} + \tfrac{1}{3}\bar{U}. \tag{4.7}$$

Recall that the gradient $\bar{S}_\chi{}^a$ includes dependence on ϕ through the coupling $\kappa(\phi)$; see eq. (2.36).

We specify the parameters of the initial shear components Z^0_{ab} and scalar field velocities Q_ϕ, Q_χ given in eqs. (3.8) and (3.9)–(3.10), respectively, such that they correspond to initial conditions with highly non-perturbative deviations from a flat FRW spacetime:

$$\xi = 0.01, \quad a_1 = 0, \quad a_2 = 0.01, \quad b_1 = -0.15, \quad b_2 = 1.8, \tag{4.8}$$

$$f_\phi = 0.5, \quad \mu_\phi = 1, \quad d_\phi = -1.7, \quad Q_0 = 0.6, \tag{4.9}$$

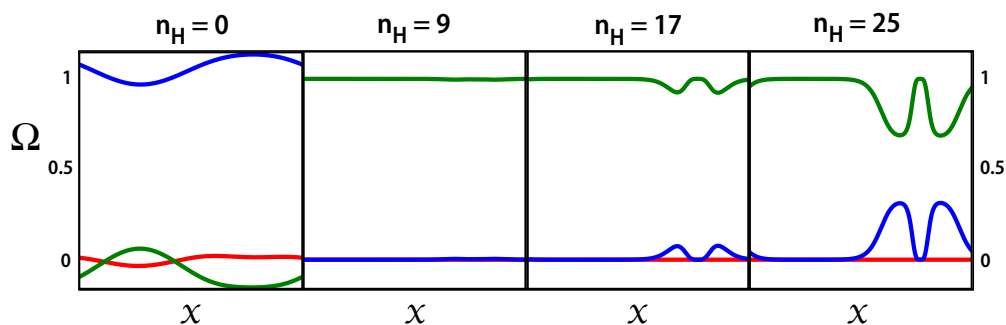$$f_\chi = 0.1, \quad \mu_\chi = 1, \quad d_\chi = -1.7. \tag{4.10}$$

Figure 1. For the case with $M = 0.2$ and $m_\chi = 0$, snapshots of the normalized energy density in $\Omega_{\phi-\chi}$ (green), spatial curvature Ω_k (red) and shear Ω_s (blue) for $0 \leq x \leq 2\pi$ at four different time steps $n_H = -t$, where n_H is the number of e-folds of contraction of the inverse mean curvature Θ.

In addition, for the three representative cases, we fix the model parameters

$$V_0 = 0.1 \text{ and } M/m = 1.015, \tag{4.11}$$

where the ratio M/m is chosen such that the predicted tilt of the temperature fluctuation spectrum matches current observations [1]. Note that for $\xi, a_1, a_2, b_1, b_2, f_\phi, \mu_\phi, d_\phi, Q_0$, and V_0, we chose the same values as in the single field case studied ref. [6], to facilitate comparison. (An extensive study with other sets of parameters and combinations of multiple modes in [9] have shown that the results for this example is representative.)

The time coordinate runs from initial time $t = 0$ (or $\Theta_0 = 3$) towards $-\infty$ (or $\Theta \to 0$). Equivalently, the time can be characterized by $n_H \equiv -t$, the number of e-folds of contraction of the inverse mean curvature Θ, where n_H runs from zero towards $+\infty$. In practice, models with a classical non-singular bounce undergo slow contraction until $n_H \approx 120$ before the bounce occurs [10]. For each example studied, the same initial data was evolved with several resolutions to confirm second order convergence; the highest resolution has 4096 points on the base level.

The three representative cases correspond to different choices for M and m_χ.

4.1 Case I: $M = 0.2$ and $m_\chi = 0$

The choice $m_\chi = 0$ is a *special case* where the action (1.5) has a shift symmetry ($\chi \to \chi +$ const.). The value of $M = 0.2$ ($\epsilon_\phi = 13$) was shown in the single field studies to be just above the minimum required for robust and rapid smoothing and flattening [6, 9]. In this case with two fields and the special shift symmetry, though, we find a different outcome.

Figure 1 shows four snapshots of the evolution of the normalized scalar field energy density $\Omega_{\phi-\chi}$ (green), spatial curvature Ω_k (red) and shear Ω_s (blue). The first snapshot ($n_H = 0$) shows the initial non-perturbative deviations from flat FRW. By the second snapshot, a short time later ($n_H = 9$), the spacetime approaches flat FRW with $\Omega_{\phi-\chi} \approx 1$ and $\Omega_s \approx \Omega_k \approx 0$, seemingly similar to the single-field case. But instead of remaining smooth and flat as found in the single-field case, something different occurs: the flat FRW phase is not stable, and the shear (blue curve) begins to grow, as illustrated in the last two snapshots. At $n_H = 25$, the geometry is spatially flat but with a mix of field energy plus shear. This combination was termed as 'Kasner-like' in the single field case [6] where it was found in certain examples with values M bigger than $0.2\, M_{\text{Pl}}$. As we will see, though, something quite
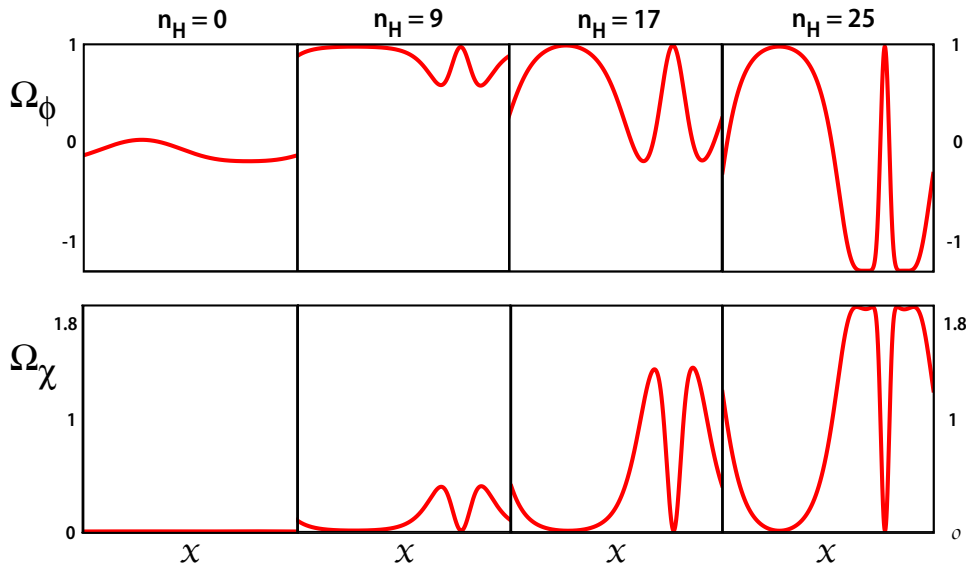
Figure 2. For the case with $M = 0.2$ and $m_\chi = 0$, snapshots of Ω_ϕ (top row) and Ω_χ (bottom row) at the same times as shown in figure 1.

different is happening in the case of two kinetically coupled fields. Note that spikes will form at locations where the χ-gradient vanishes; i.e., due to the ultralocal nature of the evolution, such points get stuck at the FRW state, whereas adjacent regions, destabilized by a non-zero χ-gradient, transition to the final Kasner-like states. Thus, using the terminology of ref. [6], the state should be referred to as 'Kasner-like (modulo spikes).'

Figure 2, which tracks the evolution of Ω_ϕ and Ω_χ separately, reveals more details. As the sequence progresses, it can be seen that Ω_ϕ rapidly comes to dominate, but then energy is transferred to χ through their non-linear coupling such that Ω_χ begins to grow. More precisely, $\bar{W}_\chi \to 0$ almost immediately, by $n_H = 2$, and remains negligible; however, the rescaled χ-gradient $\bar{S}_\chi{}^x = \sqrt{\kappa(\phi)}D^x\chi$ grows rapidly proportional to the coupling factor, $\sqrt{\kappa(\phi)}$, that is growing rapidly due to the growth of ϕ which is quickly rolling downhill its potential $V(\phi)$. (N.B. This growth of the gradient is real, i.e. not a frame effect, as explained in the appendix A.) By the last snapshot $n_H = 25$, which is far short of the bounce, Ω_χ grows to dominate over Ω_ϕ; and, then, looking back to the last snapshot in figure 1, we see that, at the same time, the gradient sources a growing shear component Ω_s. We stop the code at $n_H = 25$ for reasons described in the next section where we also use analytics to determine how the evolution continues.

4.2 Case II: $M = 0.1$ and $m_\chi = 0$

Here again we consider the *special case* with $m_\chi = 0$ in which the action (1.5) has a shift symmetry. This example illustrates that slightly decreasing M (or, equivalently, increasing the equation of state during slow contraction ϵ_ϕ) significantly delays the onset of the instability but does not eliminate it, as illustrated by this example. Figure 3 shows that the universe is rapidly flattened as in Case I, but in this case the shear Ω_s only begins to dominate for some ranges of x at $n_H = 120$. If there were no bounce and the simulation were running for a yet longer range of n_H, the behavior would be similar to the Case I but shifted in time. As a practical matter, though, by decreasing M modestly further, $M < 1/15$, the instability could
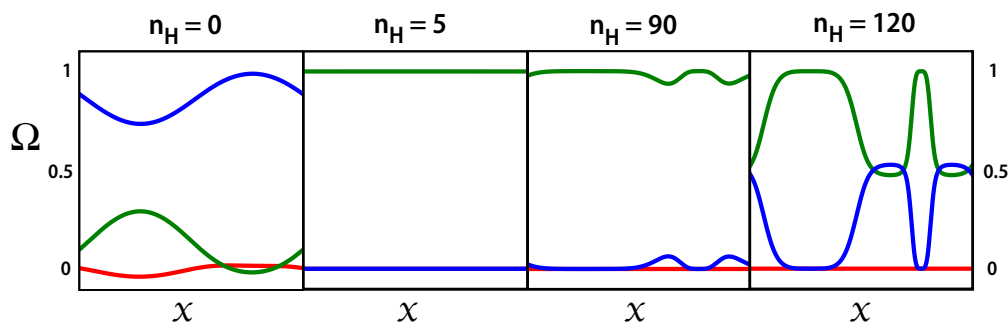
Figure 3. For the case with $M = 0.1$ and $m_\chi = 0$, snapshots of the normalized energy densities following the same color code as in figure 1. Comparing to figure 1, one observes that decreasing M, or equivalently, increasing the equation of state ϵ_ϕ of the ϕ field in eq. (1.4), rapidly and robustly drives the universe towards FRW, but a non-zero χ-gradient eventually destabilizes the FRW state.
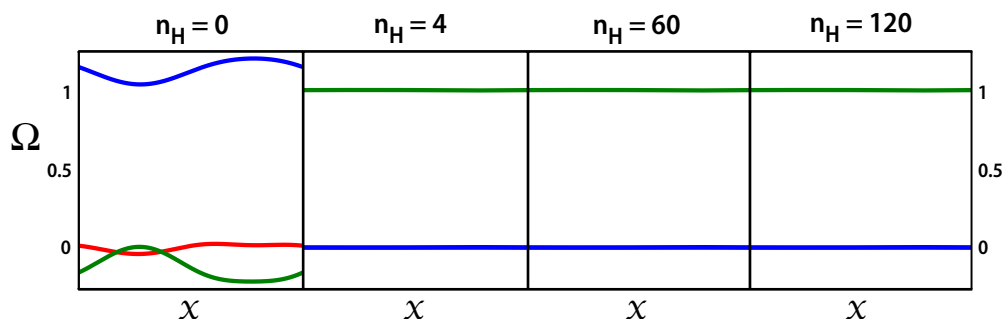

Figure 4. For the case with $M = 0.1$ and $m_\chi = 300\Theta_0^{-1}$, snapshots of the normalized energy density following the same color code as in figures 1 and 3. Compared to the case in figure 3, one observed that introducing a small m_χ suffices to obtain robust and rapid smoothing.

be delayed beyond $n_H = 120$, which is more than sufficient for bouncing cosmologies with a smooth (non-singular) bounce (where the bounce occurs at $n_H < 120$).

4.3 Case III: $M = 0.1$ and $m_\chi = 300\,\Theta_0^{-1}$

Now we turn to the *generic* case of $m_\chi \neq 0$, thus breaking the shift symmetry, which we show also acts to suppress the instability. (This case is generic because there is no reason to expect an exact shift symmetry in χ since there is no shift symmetry in ϕ.) Bearing in mind that the initial value of the inverse extrinsic curvature is $\Theta_0^{-1} \lesssim 10^{-42}\,\mathrm{GeV}$ in bouncing cosmologies, Figures 4 and 5 show that it suffices to break the shift symmetry in χ with even a small mass m_χ in order to obtain a qualitatively different result. The reason will be explained in section 5 below.

Figure 4 shows that, beginning from the same initial conditions as in Cases I and II, the geometry robustly and rapidly (by $n_H = 4$) converges to flat FRW, just as in the single field case. (A similar result is found for $M = 0.2$ for a slightly greater value of m_χ.) In particular, the gradients $\bar{S}_\chi^x$ and the shear Ω_s remain small over the $n_H = 120$ e-folds of the simulation, sufficient for practical applications to bouncing cosmologies with a gentle (non-singular) bounce.
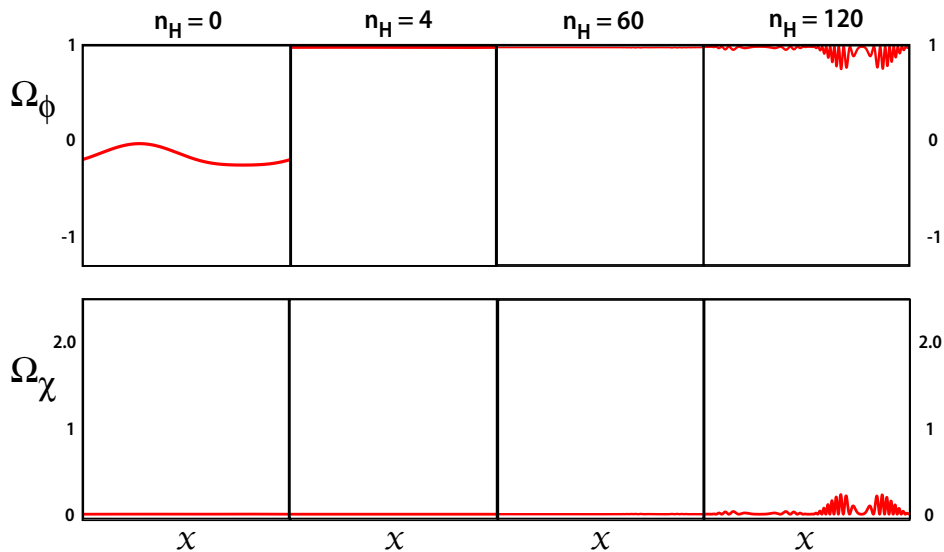
Figure 5. For the case with $M = 0.1$ and $m_\chi = 300$, snapshots of Ω_ϕ (top row) and Ω_χ (bottom row) at the same times as in figure 4.

Figure 5 shows a subtle difference from the single-field case, though. Although the total normalized scalar field energy density $\Omega_{\phi-\chi}$ is close to unity and the shear is negligible, the kinetic coupling between the two fields through the gradient $\bar{S}_\chi^x$ result in an exchange of energy between the two components, as shown by the compensating oscillations at $n_H = 120$, albeit an exchange that generates negligible shear. These can be viewed as classically generated entropic fluctuations; in this example and for a wide range of M and m_χ, these fluctuations have an amplitude that is irrelevant compared to the quantum-generated entropic fluctuations on the length scales measured by cosmic microwave background observations. Their presence is a sign that the evolution is beginning to deviate away from flat FRW; in principle, given additional time, the system would evolve to a Kasner-like fixed point as in the cases above (but this has no practical relevance for cosmologies involving a slow contraction phase that connect to the hot expanding phase through a smooth non-singular bounce.)

5   Analytic approximation

The numerical studies in the previous section show that slow contraction in the two-field models considered in this paper is in general a rapid and robust smoother over the time scales and length scales of interest for bouncing cosmologies. However, the three numerical results also show that there is a subtlety that does not arise in the case of a single canonical scalar field with a steep negative potential. Namely, a flat FRW state is not the ultimate fixed point attractor; although the evolution initially approaches a flat FRW fixed point, it is subsequently deflected towards a homogeneous but anisotropic 'Kasner-like' state.

To understand this novel phenomenon, we study different stages in the evolution using analytic perturbative analyses. These explain how the deflection from flat FRW arises and show that the characteristic time scale for the deflection is in general of $\mathcal{O}(100)$ or more e-foldings of contraction of the inverse mean curvature, which is of no practical relevance in cosmologies where slow contraction connects to the hot expansion phase through a smooth classical (non-singular) bounce.

The evolution beginning from highly non-perturbative deviations from flat FRW involves four stages:

Stage 1. During the first stage, the system evolves from the freely specified initial state (as detailed above in section 3) to one that is *ultralocal*, meaning that terms involving spatial derivatives (gradients) are quickly dominated by velocity terms (i.e., terms that do not involve spatial derivatives) as the evolution proceeds. In particular, within only a few *e*-folds of contraction of the inverse mean curvature Θ,

$$\bar{E}_a{}^i \to 0, \ \bar{A}_b \to 0, \ D_a\phi \to 0, \ D_a\chi \to 0. \tag{5.1}$$

Note that ultralocal does not mean flat FRW, as extensively detailed in ref. [11].

Stage 2. For $M \leq 0.2$ and $Q_0 > 0$, the same range considered in ref. [6], the Einstein-scalar system (2.18)–(2.27) rapidly and non-linearly evolves from an ultralocal (but not FRW) state towards the flat FRW stationary point with

$$\bar{W}_\chi \simeq 0, \bar{S}_\chi{}^a \simeq 0, \bar{U}_{,\chi} \simeq 0, \tag{5.2}$$

$$\bar{n}_{ab} \simeq 0, \ \bar{\Sigma}_{ab} \simeq 0, \ \bar{W}_\phi \simeq M^{-1}, \ \bar{V} \simeq 3 - \frac{1}{2}M^{-2}, \ \mathcal{N} \simeq 2M^2, \tag{5.3}$$

just as we observe by $n_H = 9$ in all of our simulations as illustrated in the second panels of figures 1, 3 and 4.

The first two stages are very rapid (complete by $n_H \lesssim 10$) and are determined by the slow contraction sourced by the ϕ-field. As result, the evolution during these two stages is similar to what is found for the single-field case.

Stage 3. For the case of a single canonical scalar, flat FRW is a stable fixed point of the evolution. For the kinetically-coupled two-field models considered here, though, flat FRW is *not* a stable fixed point. Rather, there remain small deviations from flat FRW that eventually grow large enough to deflect the evolution from the flat FRW fixed point. This effect can be seen by perturbing the Einstein-scalar system of equations (2.18)–(2.27) around the flat FRW fixed point given by eqs. (5.2)–(5.3).

Inspecting the linearized system,

$$\partial_t \delta\bar{E}_a{}^i = \left(1 - \mathcal{N}\right)\delta\bar{E}_a{}^i, \tag{5.4}$$

$$\partial_t \delta\bar{A}_b = \left(1 - \mathcal{N}\right)\delta\bar{A}_b, \tag{5.5}$$

$$\partial_t \delta\bar{n}^{ab} = \left(1 - \mathcal{N}\right)\delta\bar{n}^{ab}, \tag{5.6}$$

$$\partial_t \delta\bar{\Sigma}_{ab} = \left(1 - 3\mathcal{N}\right)\delta\bar{\Sigma}_{ab}, \tag{5.7}$$

$$\partial_t \delta\bar{W}_\phi = \left(1 - 3\mathcal{N}\right)\delta\bar{W}_\phi - \left(3\bar{W}_\phi - M^{-1}\bar{V}\right)\delta\mathcal{N} + M^{-1}\mathcal{N}\delta\bar{V}, \tag{5.8}$$

$$\partial_t \delta\bar{S}_{\phi x} = \left(1 - \mathcal{N}\right)\delta\bar{S}_{\phi x}, \tag{5.9}$$

$$\partial_t \delta\chi = \mathcal{N}\,\frac{\delta\bar{W}_\chi}{\sqrt{\kappa(\phi)}} \tag{5.10}$$

$$\partial_t \delta \bar{W}_\chi = \left(1 - \mathcal{N} \left(3 - \frac{1}{2} m^{-1} \bar{W}_\phi \right) \right) \delta \bar{W}_\chi - \mathcal{N} \frac{\bar{U}_{,\chi\chi}}{\sqrt{\kappa} 1} \delta \chi, \tag{5.11}$$

$$\partial_t \delta \bar{S}_{\chi x} = \left(1 - \mathcal{N} \left(1 + \frac{1}{2} m^{-1} \bar{W}_\phi \right) \right) \delta \bar{S}_{\chi x}, \tag{5.12}$$

where δ denotes linear perturbations around the background solutions, it is immediately apparent that the perturbations of all geometric variables as well as the linearized scalar field variables $\delta \bar{W}_\phi, \delta \bar{S}_{\phi a}$ form a closed system and decay at the same rate as in the single field case as $|t|$ grows, i.e.,

$$\delta \bar{E}_a{}^i, \delta \bar{A}_b, \delta \bar{n}^{ab}, \delta \bar{S}_{\phi x} \propto e^{(1-2M^2) t}, \tag{5.13}$$

$$\delta \bar{\Sigma}^{ab}, \delta \bar{W}_\phi \propto e^{(1-6M^2) t}, \tag{5.14}$$

where $\mathcal{N} = 2M^2 \leq 2/5.2^2$; see eq. (5.3). Hence the exponents $1 - \mathcal{N} \geq 0.93$, $1 - 3\mathcal{N} \geq 0.78$ are both positive definite, in agreement with the results found in ref. [6]. (Positive exponents correspond to decay because the time variable runs from 0 towards $t \to -\infty$.)

Solving the linearized equations (5.10)–(5.11) around the flat FRW stationary point (5.3), it is straightforward to verify that the kinetic interaction $\kappa(\phi) = e^{-\phi/m}$ makes the $\bar{W}_\chi = 0$ solution stable. In matrix form, the closed system can be written as

$$\partial_t \begin{pmatrix} \delta \chi \\ \delta \bar{W}_\chi \end{pmatrix} = \begin{pmatrix} 0 & 2M^2/\sqrt{\kappa(\phi)} \\ -2M^2 \bar{m}_\chi^2/\sqrt{\kappa(\phi)} & 1 - 6M^2 + M/m \end{pmatrix} \begin{pmatrix} \delta \chi \\ \delta \bar{W}_\chi \end{pmatrix}. \tag{5.15}$$

The two eigenvalues $\lambda_\pm$ corresponding to the coefficient matrix are given by

$$\lambda_\pm = \frac{1}{2} \left(1 - 6M^2 + M/m \right) \left(1 \pm \sqrt{1 - \frac{16 \bar{m}_\chi^2 M^4}{\kappa(\phi)(1 - 6M^2 + M/m)^2}} \right) \tag{5.16}$$

$$\simeq \left(1 - 3M^2 \right) \left(1 \pm \sqrt{1 - \frac{0.8 m_\chi^2 M^6 e^{2t}}{(1 - 6M^2)(1 - 3M^2)^2}} \right), \tag{5.17}$$

where we substituted $\bar{V}_0 = 0.1$ and $M/m = 1.015$ as defined in eq. (4.11) and used $\kappa(\phi) = (-\bar{V}/\bar{V}_0)^{M/m}$ to evaluate $\kappa(\phi)$ at the flat FRW stationary point. Note that the second term under the square root is positive for $M \leq 0.2$ and $m_\chi = 300 \Theta_0{}^{-1}$, which means that the kinetic energy density is stable even for $m_\chi = 0$; the term becomes vanishingly small as $t \to -\infty$.

Although the analysis to this point might suggest that the flat FRW fixed point is stable, there remains the (rescaled) spatial gradient of χ to consider, which turns out to be the source of the instability. More precisely, the same factor $\kappa(\phi)$ that stabilizes the time derivative of χ destabilizes the $\bar{S}_\chi{}^x \simeq 0$ gradient contribution: evaluating the evolution equation (5.12) of $\bar{S}_\chi{}^x$ for the flat FRW stationary point solution in eq. (5.3),

$$\partial_t \delta \bar{S}_\chi{}^x \simeq \left(1 - 2M^2 - M/m \right) \delta \bar{S}_\chi{}^x, \tag{5.18}$$

with $M/m = 1.015$, it becomes apparent that the gradient perturbation slowly grows,

$$\delta \bar{S}_\chi{}^x = \delta \bar{S}_\chi{}^x(t_{\mathrm{FRW}}) e^{-(0.015 + 2M^2) t}, \tag{5.19}$$

where $\delta \bar{S}_\chi{}^x(t_{\mathrm{FRW}})$ is the value of $\delta \bar{S}_\chi{}^x$ at the beginning of Stage 3, when the flat FRW stage begins. The system non-linearly approaches the flat FRW fixed point solution. This

expression is valid at the linear level during Stage 3; the small entropic fluctuations shown in the last panel of figure 5 arise as non-linear gradient effects on the evolution grow to become non-negligible. Note that the time scale of the instability does not depend on m_χ; the role of a non-zero m_χ is to drive the χ field towards the minimum of its potential energy density, thereby reducing it gradient, $\delta \bar{S}_\chi{}^x(t_{\rm FRW})$, by many orders of magnitude and extending the time scale before the instability has a significant effect.

Stage 4. $\bar{S}_\chi{}^x$ eventually grows large enough to deflect the evolution away from flat FRW and towards the stable Kasner-like fixed point with a time-invariant, non-zero $\delta \bar{S}_\chi{}^x$ where

$$\mathcal{N}^{-1} = \frac{6 - 3\,M/m}{3(M/m)^2 - 5\,M/m + 2 + 8M^2}, \tag{5.20}$$

$$\bar{W}_\chi = 0, \tag{5.21}$$

$$\bar{S}_{\chi x}^2 = 2\,\mathcal{N}^{-2} \times \frac{\left(3(M/m)^2 - 4\,M/m + 8M^2\right)\left(1 - M/m - 2M^2\right)}{(2 - M/m)^2}, \tag{5.22}$$

$$\bar{n}_{ab} = 0 \quad \text{for all} \quad a, b, \tag{5.23}$$

$$\bar{\Sigma}_{xx} = -\frac{2}{3} \times \frac{\bar{S}_{\chi x}^2}{\mathcal{N}^{-1} - 3}, \tag{5.24}$$

$$\bar{\Sigma}_{yy} = \bar{\Sigma}_{zz} = -\frac{1}{2} \times \bar{\Sigma}_{xx}, \tag{5.25}$$

$$\bar{\Sigma}_{ab} = 0 \quad \text{for all} \quad a \neq b, \tag{5.26}$$

$$\bar{W}_\phi = 2\,m \times \left(\mathcal{N}^{-1} - 1 - \bar{\Sigma}_{xx}\right), \tag{5.27}$$

$$\bar{V}(\phi) = -M \times \left(\frac{m^{-1}}{2} \times \bar{S}_{\chi x}^2 + (\mathcal{N}^{-1} - 3)\bar{W}_\phi\right). \tag{5.28}$$

As we show in appendix B, the Kasner-like stationary point corresponds to a state with a time-independent non-zero gradient, the true attractor solution for combinations of m_χ, M, and m employed in our studies.

Eq. (5.19) is a key result: it tells us that the characteristic duration of Stage 3 (i.e., the period where the evolution remains close to the unstable flat FRW fixed point) is of $\mathcal{O}(\frac{1}{0.015+2M^2})$, which can be more than one hundred e-foldings for values of M that are not pushed too close to the Planck scale and for even small values of m_χ, as shown in the example in figure 4. The precise duration depends on the value of $\delta \bar{S}_\chi{}^x(t_{\rm FRW})$, the magnitude of $\delta \bar{S}_\chi{}^x$ at the beginning of Stage 3. The value depends on the initial conditions and the non-linear evolution that takes places in Stages 1 and 2, which can only be determined by evolving the system of equations using full numerical relativity. The important point, though, is that Stage 3, the flat FRW phase, endures sufficiently long for values of M and m_χ characteristic of bouncing cosmologies with a smooth (non-singular) bounce; the later instability is irrelevant because the bounce would occur while the spacetime is still close to the flat FRW state.

6 Discussion

Using the tools of numerical general relativity, we studied the cosmological evolution during slow contraction in models where the stress-energy is sourced by two kinetically-coupled scalar fields with an exponential non-linear σ model-type interaction beginning from inhomogeneous

and anisotropic initial conditions that deviate far from flat FRW spacetimes. Our main finding was that slow contraction led to a robust and rapid convergence to a flat FRW geometry, similar to previous results obtained in refs. [3, 6, 11] for the case where slow contraction is sourced by a single canonical scalar field.

However, our study revealed a subtle difference as well. Whereas the flat FRW solution is a stable attractor in the single-field case, it is not in the case of the two kinetically coupled fields considered here. Instead, the evolution in the two-field case rapidly becomes ultralocal and approaches close to the flat FRW fixed point where it remains for a considerable period, but ultimately it is deflected away from that fixed point and towards a Kasner-like fixed point. We investigated the instability analytically and showed that the characteristic time for the instability to develop enough to cause the deflection is $\mathcal{O}(100)$ or more e-folds of contraction of the inverse mean curvature Θ.

In addition, we showed that slightly decreasing the characteristic scale M of the negative exponential potential $\bar{V} = -\bar{V}_0 e^{-\phi/M}$ associated with the field ϕ that drives slow contraction as well as increasing the mass $\bar{m}_\chi$ of the light χ field which couples to ϕ through a non-linear σ type kinetic interaction further increases the duration of the flat FRW period and delays the deflection to the Kasner-like fixed point.

The result is reminiscent of the single-field case discussed in ref. [9] where, for some initial data sets, we found that the system first evolved close to a Kasner-like fixed point before it was deflected to the stable flat FRW attractor solution. There are two key differences between the two cases, though:

- in the single field case, the system approaches close to the (unstable) Kasner-like fixed point for only a *very small subset of initial conditions* and it remains there for only a *short period* before being deflected to the stable attractor fixed point (the flat FRW state),

- in the kinetically-coupled two-field case, the system approaches close to the (unstable) flat FRW fixed point for a *very wide range of initial conditions* and remains there for a *long period* before being deflected to the stable attractor Kasner-like fixed point.

This result is surprising and was not anticipated in previous studies based on the conventional perturbative techniques commonly applied in cosmology. Hence, this study is a fine demonstration of the power of non-perturbative, numerical relativity to reveal novel cosmological dynamics that one could not anticipate through conventional perturbative methods but that are critically important to understand in developing cosmological models.

In the present example, the difference between the single-field and kinetically-coupled two-field case turns out not to be observationally relevant in bouncing cosmologies because the end of slow contraction and the transition to the hot expanding phase begins around 100 e-foldings of contraction of Θ — before the flat FRW state destabilizes. This is significant because the kinetically-coupled two-field models studied here are examples that can generate a nearly scale-invariant spectrum of super-Hubble density fluctuations fully consistent with cosmic microwave background observations.

Acknowledgments

A Tetrad frame transformation rules

In this appendix, we consider the relationship between geometric variables as represented in the hypersurface-orthogonal tetrad frame (used in our tetrad codes to study smoothing of initial conditions) and the co-moving tetrad frame. To this end, we will first derive the transformation rules for the tetrad vector components, the Ricci rotation coefficients and the (effective) 'fluid' variables describing the stress-energy under the Lorentz boost $\{\Lambda_\alpha{}^\beta\}$ that connects two arbitrary tetrad frames. Then, we apply the rules to the case of scalar fields to transform geometric and 'fluid' variables from the hypersurface-orthogonal tetrad frame to the co-moving tetrad frame.

We are interested in tetrad frame transformations under Lorentz boosts $\{\Lambda_\alpha{}^\beta\}$ that transform a time-like tetrad $\mathbf{e_0}$ to another $\tilde{\mathbf{e}}_0$. The boost is defined through the rapidity β between the two 4-vectors $\mathbf{e_0}$ and $\tilde{\mathbf{e}}_0$ and through the projection $\{w_a\}$ of $\tilde{\mathbf{e}}_0$ into the 3-surfaces spanned by the spatial triad $\mathbf{e_a}$ $(a = 1, 2, 3)$:

$$\Lambda_0{}^0 \equiv \cosh\beta, \quad \Lambda_a{}^0 \equiv \sinh\beta\, w_a, \quad \Lambda_a{}^b = w_a w^b(\cosh\beta - 1) + \delta_a{}^b, \tag{A.1}$$

where $w_a w^a = 1$. Note that $\Gamma \equiv \cosh\beta = 1/\sqrt{1 - \mathbf{v}^2}$ is the Lorentz factor with $v_a \equiv \tanh\beta\, w_a$. In particular,

$$\Lambda_0{}^0 = \Gamma, \quad \Lambda_a{}^0 = \Gamma v_a, \quad \Lambda_a{}^b = \frac{\Gamma^2}{\Gamma + 1} v_a v^b + \delta_a{}^b. \tag{A.2}$$

Vierbein. The tetrad frame vectors $\{e_\alpha\}$ and $\{\tilde{e}_\alpha\}$ (with $\alpha = 0, \ldots, 3$) are related as follows:

$$\tilde{e}_0 = \Lambda_0{}^\beta \mathbf{e}_\beta = \Gamma\Big(\mathbf{e}_0 + v^b \mathbf{e}_b\Big), \tag{A.3}$$

$$\tilde{e}_a = \Lambda_a{}^\beta e_\beta = \Gamma v_a \mathbf{e}_0 + \Big(\delta_a{}^b + \frac{\Gamma^2}{\Gamma + 1} v_a v^b\Big)\mathbf{e}_b. \tag{A.4}$$

Ricci Rotation Coefficients. The Ricci Rotation Coefficients $\gamma_{\alpha\beta\lambda}$ which are defined as

$$\gamma_{\alpha\beta\lambda} \equiv e_\alpha \nabla_\lambda e_\beta, \tag{A.5}$$

with $\nabla_\lambda \equiv e_\lambda{}^\mu \nabla_\mu$ transform as follows:

$$\tilde{\gamma}_{\alpha\beta\lambda} = \tilde{e}_\alpha \tilde{\nabla}_\lambda \tilde{e}_\beta = \tilde{e}_\alpha \tilde{e}_\lambda{}^\mu \tilde{\nabla}_\mu \tilde{e}_\beta = \Lambda_\alpha{}^\delta e_\delta \Lambda_\lambda{}^\zeta e_\zeta{}^\mu \nabla_\mu \left(\Lambda_\beta{}^\epsilon e_\epsilon\right) \tag{A.6}$$
$$= \Lambda_\alpha{}^\delta \Lambda_\beta{}^\epsilon \Lambda_\lambda{}^\zeta \gamma_{\delta\epsilon\zeta} - \eta_{\delta\epsilon} \Lambda_\beta{}^\epsilon \Lambda_\lambda{}^\zeta \nabla_\zeta \Lambda_\alpha{}^\delta.$$

Components of the Stress-Energy Tensor. Characterizing an arbitrary stress-energy tensor through effective 'fluid' variables,

$$\varrho \equiv e_0{}^\mu e_0{}^\nu T_{\mu\nu}, \tag{A.7}$$

$$j_a \equiv -e_0{}^\mu e_a{}^\nu T_{\mu\nu}, \tag{A.8}$$

$$s_{ab} \equiv \pi_{ab} + p\delta_{ab} \equiv e_a{}^\mu e_b{}^\nu T_{\mu\nu}, \tag{A.9}$$

$$p \equiv \tfrac{1}{3} s_a{}^a, \tag{A.10}$$

where ϱ is the energy density, j_a the three-momentum flux, s_{ab} the spatial stress tensor and p denotes the pressure and π_{ab} denotes the trace-free anisotropic stress (with $\pi_{ab} \equiv s_{(ab)} - \frac{1}{3}s_a{}^a\delta_{ab}$), under a Lorentz boost as defined in eq. (A.1), the 'fluid' variables transform as follows:

$$\tilde{T}_{\alpha\beta} = \tilde{e}_\alpha{}^\mu\tilde{e}_\beta{}^\nu T_{\mu\nu} = \Lambda_\alpha{}^\gamma\Lambda_\beta{}^\delta e_\gamma{}^\mu e_\delta{}^\nu T_{\mu\nu} \tag{A.11}$$
$$= \Lambda_\alpha{}^0\Lambda_\beta{}^0\rho - \Lambda_\alpha{}^0\Lambda_\beta{}^a j_a - \Lambda_\alpha{}^b\Lambda_\beta{}^0 j_b + \Lambda_\alpha{}^a\Lambda_\beta{}^b s_{ab},$$

i.e.,

$$\tilde{\varrho} = \Gamma^2\varrho - 2\Gamma^2 j_a v^a + \Gamma^2 v^a v^b s_{ab}, \tag{A.12}$$

$$\tilde{j}_a = -\Gamma^2\varrho v_a + \Gamma j_a + \Gamma^2\left(1 + \frac{\Gamma}{\Gamma+1}\right)j_b v^b v_a - \Gamma\left(\delta_a{}^c + \frac{\Gamma^2}{\Gamma+1}v_a v^c\right)v^b s_{bc}, \tag{A.13}$$

$$\tilde{s}_{ab} = s_{ab} + \Gamma^2\varrho v_a v_b - \Gamma\left(v_a j_b + v_b j_a\right) - 2\frac{\Gamma^3}{\Gamma+1}v^c j_c v_a v_b + \frac{\Gamma^4}{(\Gamma+1)^2}v^c v^d s_{cd}v_a v_b \tag{A.14}$$
$$+ \frac{\Gamma^2}{\Gamma+1}\left(v_b v^c s_{ac} + v_a v^c s_{cb}\right).$$

For the numerical relativity codes that we use to study the robustness and rapidity of slow contraction, we fixed the tetrad frame gauge to be hypersurface-orthogonal and Fermi propagated, as described in section 2.2. In particular, the timelike vierbein $\mathbf{e_0}$ is normal to spacelike hypersurfaces. In general, $j_a \neq 0$ in this frame, which means that, typically, $\mathbf{e_0}$ and the effective fluid's 4-velocity (which is the timelike congruence $\tilde{\mathbf{e}}_0$ of the co-moving tetrad) do not coincide.

For example, in the case of a single scalar field, where

$$T_{\mu\nu} = \nabla_\mu\phi\nabla_\nu\phi - \left(\tfrac{1}{2}\nabla_\mu\phi\nabla^\mu\phi + V(\phi)\right)g_{\mu\nu}, \tag{A.15}$$

the 'fluid' variables ϱ, j_a, s_{ab}, and p in the hypersurface-orthogonal tetrad frame take the following form:

$$\varrho = \tfrac{1}{2}D_0\phi D_0\phi + \tfrac{1}{2}D_a\phi D^a\phi + V(\phi), \tag{A.16}$$

$$j_a = -D_0\phi D_a\phi, \tag{A.17}$$

$$s_{ab} = D_a\phi D_b\phi + \left(\tfrac{1}{2}D_0\phi D_0\phi - \tfrac{1}{2}D_c\phi D^c\phi - V(\phi)\right)\delta_{ab}, \tag{A.18}$$

$$p = \tfrac{1}{2}D_0\phi D_0\phi - \tfrac{1}{6}D_c\phi D^c\phi - V(\phi). \tag{A.19}$$

Here, D_0 denotes the Lie derivative along e_0 and D_a is the directional derivative along e_a. Manifestly, $\mathbf{e_0} \neq -D_a\phi/D_0\phi$ ad hence the hypersurface-orthogonal and co-moving tetrad frames do not coincide in general. The Lorentz boost, $v_a = -D_a\phi/D_0\phi$, transforms the tetrad to the co-moving frame, where the stress-energy takes the form of a perfect fluid:

$$\tilde{\varrho} = \tfrac{1}{2}D_0\phi D_0\phi + \tfrac{1}{2}D_c\phi D^c\phi - V(\phi), \quad \tilde{p} = \tfrac{1}{2}D_0\phi D_0\phi - \tfrac{1}{2}D_c\phi D^c\phi - V(\phi), \tag{A.20}$$

$$j_a = \pi_{ab} = 0. \tag{A.21}$$

Note, though, that the hypersurface-orthogonal tetrad frame converges to the co-moving frame if $v_a = (D_a\phi/\dot\phi) \to 0$, as is the case in our simulations that involve a single scalar

which is minimally-coupled to gravity and has a negative potential. By contrast, our initial data as specified above in section 3 is *not* represented in the co-moving frame. This does not affect the conclusion that the spacetime converges to a homogeneous, isotropic and spatially flat FRW universe. However, it does mean that the initial conditions are not as a Eulerian co-moving observer would measure them to be.

More generally, the Lorentz boost $v_a = j_a/(\varrho + p_c)$ with p_c being the co-moving pressure transforms an arbitrary tetrad frame to the co-moving frame. If, in addition, $s_{ab} = j_a j_b + p_c \delta_{ab}$, it is straightforward to show that the 'fluid' takes the perfect fluid form in the co-moving tetrad frame with

$$\tilde{\varrho} = \frac{1}{\Gamma^2}(\varrho + p_c) - p_c, \quad \tilde{s}_{ab} = p_c \delta_{ab}, \quad j_a = \pi_{ab} = 0. \tag{A.22}$$

In the case of two kinetically-interacting scalars like those considered in this paper with

$$T_{\mu\nu} = \nabla_\mu \phi \nabla_\nu \phi + \kappa(\phi)\nabla_\mu \chi \nabla_\nu \chi - \left(\tfrac{1}{2}\nabla_\mu \phi \nabla^\mu \phi + \tfrac{1}{2}\kappa(\phi)\nabla_\mu \chi \nabla^\mu \chi + V(\phi) + U(\chi)\right)g_{\mu\nu}, \tag{A.23}$$

the 'fluid' variables ϱ, j_a, s_{ab}, and p in the hypersurface-orthogonal tetrad frame take the following form:

$$\varrho = \tfrac{1}{2}\left(D_0\phi D_0\phi + D_a\phi D^a\phi\right) + V(\phi) + \tfrac{1}{2}\kappa(\phi)\left(D_0\chi D_0\chi + D_a\chi D^a\chi\right) + U(\chi), \tag{A.24}$$

$$j_a = -D_0\phi D_a\phi - \kappa(\phi)D_0\chi D_a\chi, \tag{A.25}$$

$$s_{ab} = D_a\phi D_b\phi + \kappa(\phi)D_a\chi D_b\chi \tag{A.26}$$
$$\quad + \left(\tfrac{1}{2}\left(D_0\phi D_0\phi - D_c\phi D^c\phi\right) - V(\phi) + \tfrac{1}{2}\kappa(\phi)(D_0\chi D_0\chi - D_c\chi D^c\chi) - U(\chi)\right)\delta_{ab},$$

$$p = \tfrac{1}{2}\left(D_0\phi D_0\phi - \tfrac{1}{3}D_c\phi D^c\phi\right) - V(\phi) + \tfrac{1}{2}\kappa(\phi)\left(D_0\chi D_0\chi - \tfrac{1}{3}D_c\chi D^c\chi\right) - U(\chi). \tag{A.27}$$

Again, it is immediately apparent from eq. (A.25) that the hypersurface orthogonal and the co-moving frames do not coincide.

The Lorentz boost defined through

$$v_a = -\frac{D_0\phi D_a\phi + \kappa(\phi)D_0\chi D_a\chi}{D_0\phi D_0\phi + \kappa(\phi)D_0\chi D_0\chi} = \frac{j_a}{\rho + p_c} \tag{A.28}$$

transforms the hypersurface-orthogonal tetrad to the co-moving frame. Here, the co-moving pressure is defined as

$$p_c \equiv \tfrac{1}{2}\left(D_0\phi D_0\phi - D_c\phi D^c\phi\right) - V(\phi) + \tfrac{1}{2}\kappa(\phi)\left(D_0\chi D_0\chi - D_c\chi D^c\chi\right) - U(\chi), \tag{A.29}$$

and the co-moving 'fluid' variables take the following form:

$$\tilde{\varrho} = \rho + (1 - \Gamma^2)(\rho + p_c) + \Gamma^2\left(D^a\phi D^b\phi + \kappa(\phi)D^a\chi D^b\chi\right)\frac{j_a j_b}{(\rho + p_c)^2}, \tag{A.30}$$

$$\tilde{j}_a = (\Gamma^2 - 1)j_a - \Gamma\left(D_a\phi D^b\phi + \kappa(\phi)D_a\chi D^b\chi\right)\frac{j_b}{\rho + p_c} \tag{A.31}$$
$$\quad - \frac{\Gamma^3}{\Gamma + 1}\left(D^b\phi D^c\phi + \kappa(\phi)D^b\chi D^c\chi\right)\frac{j_b j_c j_a}{(\rho + p_c)^3},$$

– 21 –

$$\tilde{s}_{ab} = p_c \delta_{ab} + D_a\phi D_b\phi + \kappa(\phi)D_a\chi D_b\chi - \Gamma^2 \frac{j_a j_b}{\rho + p_c} \tag{A.32}$$

$$+ \frac{\Gamma^2}{\Gamma+1}\left((D_b\phi D^c\phi + \kappa(\phi)D_b\chi D^c\chi)\frac{j_c j_a}{(\rho+p_c)^2} + (D_a\phi D^c\phi + \kappa(\phi)D_a\chi D^c\chi)\frac{j_c j_b}{(\rho+p_c)^2}\right)$$

$$+ \frac{\Gamma^4}{(\Gamma+1)^2}(D^c\phi D^d\phi + \kappa(\phi)D^c\chi D^d\chi)\frac{j_c j_d j_a j_b}{(\rho+p_c)^4}\,.$$

In general, interacting scalar fields act as 'imperfect fluids' with non-zero momentum flux and non-diagonal spatial stress tensor.

In our studies, we found that all solutions evolve towards stationary points with

- a homogeneous ϕ profile, i.e., $D_a\phi \equiv 0$ for all $a \in \{1,2,3\}$; and

- a non-dynamical χ profile, i.e., $D_0\chi \equiv 0$.

Accordingly, for all solutions, v_a as defined in eq. (A.28) evolves to zero. This means, the hypersurface orthogonal frame evolves towards the co-moving frame such that all geometric and 'fluid' variables in the hypersurface-orthogonal frame faithfully represent the Eulerian observer's measurements. In particular,

$$\rho \to \tilde{\varrho} = \tfrac{1}{2}D_0\phi D_0\phi + V(\phi) + \tfrac{1}{2}\kappa(\phi)D_a\chi D^a\chi + U(\chi), \tag{A.33}$$

$$j_a \to \tilde{j}_a = 0, \tag{A.34}$$

$$s_{ab} \to \tilde{s}_{ab} = p_c\delta_{ab} + \kappa(\phi)D_a\chi D_b\chi\,. \tag{A.35}$$

B Dynamical stability of the fixed point solution with $\bar{S}_\chi{}^x \neq 0, \partial_t \bar{S}_\chi{}^x = 0$

To analyze the stability of the new stationary solution, we linearize the Einstein-scalar system (2.18)–(2.27) around the fixed point solution given in eq. (5.20):

$$\partial_t \delta\bar{E}_a{}^i = \left(1 - \mathcal{N}(1 + \bar{\Sigma}_{aa})\right)\delta\bar{E}_a{}^i, \tag{B.1}$$

$$\partial_t \delta\bar{A}_b = \left(1 - \mathcal{N}(1 + \bar{\Sigma}_{bb})\right)\delta\bar{A}_b, \tag{B.2}$$

$$\partial_t \delta\bar{n}_{ab} = \left(1 - \mathcal{N}(1 - \bar{\Sigma}_{aa} - \bar{\Sigma}_{bb})\right)\delta\bar{n}_{ab}, \tag{B.3}$$

$$\partial_t \delta\bar{\Sigma}_{xx} = \left(1 - 3\mathcal{N}\right)\delta\bar{\Sigma}_{xx} - \left(3\bar{\Sigma}_{xx} - \frac{2}{3}(\bar{S}_\chi{}^x)^2\right)\delta\mathcal{N} + \frac{4}{3}\mathcal{N}\bar{S}_\chi{}^x\delta\bar{S}_\chi{}^x, \tag{B.4}$$

$$\partial_t \delta\bar{\Sigma}_{yy} = \left(1 - 3\mathcal{N}\right)\delta\bar{\Sigma}_{yy} - \left(3\bar{\Sigma}_{yy} + \frac{1}{3}(\bar{S}_\chi{}^x)^2\right)\delta\mathcal{N} - \frac{2}{3}\mathcal{N}\bar{S}_\chi{}^x\delta\bar{S}_\chi{}^x, \tag{B.5}$$

$$\partial_t \delta\bar{\Sigma}_{xy} = \left(1 - 3\mathcal{N}\right)\delta\bar{\Sigma}_{xy}, \tag{B.6}$$

$$\partial_t \delta\bar{W}_\phi = \left(1 - 3\mathcal{N}\right)\delta\bar{W}_\phi + \mathcal{N}\left(M^{-1}\delta\bar{V} + m^{-1}\bar{S}_\chi{}^x\delta\bar{S}_\chi{}^x\right) \tag{B.7}$$

$$- \left(3\bar{W}_\phi - M^{-1}\bar{V} - \frac{1}{2}m^{-1}(\bar{S}_\chi{}^x)^2\right)\delta\mathcal{N},$$

$$\partial_t \delta\chi = \mathcal{N}\frac{\delta\bar{W}_\chi}{\sqrt{\kappa(\phi)}}, \tag{B.8}$$

$$\partial_t \delta\bar{W}_\chi = \left(1 - \mathcal{N}\left(3 - \frac{1}{2}m^{-1}\bar{W}_\phi\right)\right)\delta\bar{W}_\chi - \mathcal{N}\frac{\bar{U}_{,\chi\chi}}{\sqrt{\kappa}}\delta\chi, \tag{B.9}$$

$$\partial_t \delta \bar{S}_\chi{}^x = \left(1 - \mathcal{N}\left(1 + \frac{1}{2}m^{-1}\bar{W}_\phi + \bar{\Sigma}_{xx}\right)\right)\delta \bar{S}_\chi{}^x - \mathcal{N}\bar{S}_\chi{}^x\left(\frac{1}{2}m^{-1}\delta\bar{W}_\phi + \delta\bar{\Sigma}_{xx}\right) \quad \text{(B.10)}$$
$$- \left(1 + \frac{1}{2}m^{-1}\bar{W}_\phi + \bar{\Sigma}_{xx}\right)\bar{S}_\chi{}^x\delta\mathcal{N}$$

with $\delta\mathcal{N}$ and $\delta\bar{V}(\phi)$ being given through the linearized lapse equation and Hamiltonian constraint:

$$\delta\bar{V}(\phi) = -\bar{\Sigma}_{xx}\left(\delta\bar{\Sigma}_{xx} - \delta\bar{\Sigma}_{yy}\right) - \bar{W}_\phi\delta\bar{W}_\phi - \bar{S}_\chi{}^x\delta\bar{S}_\chi{}^x, \quad \text{(B.11)}$$

$$\delta\mathcal{N} = -\mathcal{N}^2\left(\bar{\Sigma}_{xx}\left(\delta\bar{\Sigma}_{xx} - \delta\bar{\Sigma}_{yy}\right) + \bar{W}_\phi\delta\bar{W}_\phi + \frac{1}{3}\bar{S}_\chi{}^x\delta\bar{S}_\chi{}^x\right). \quad \text{(B.12)}$$

For $M/m = 1.015$ and $M \leq 0.2$, the stationary point solution given in eq. (5.20) can be approximated as follows:

$$\mathcal{N} \approx \frac{8}{3} \times M^2, \quad \text{(B.13)}$$

$$\bar{W}_\chi = 0, \quad \text{(B.14)}$$

$$\bar{S}_\chi{}^x \approx \frac{3}{4} \times M^{-1}, \quad \text{(B.15)}$$

$$\bar{n}_{ab} = 0 \text{ for all } a, b, \quad \text{(B.16)}$$

$$\bar{\Sigma}_{xx} \approx -\left(1 + 0.005M^{-2}\right), \quad \text{(B.17)}$$

$$\bar{\Sigma}_{yy} = \bar{\Sigma}_{zz} \approx \frac{1}{2} \times \left(1 + 0.005M^{-2}\right), \quad \text{(B.18)}$$

$$\bar{\Sigma}_{ab} = 0 \text{ for all } a \neq b, \quad \text{(B.19)}$$

$$\bar{W}_\phi \approx \frac{3}{4} \times M^{-1}, \quad \text{(B.20)}$$

$$\bar{V}(\phi) \approx -\frac{9}{16}\left(M^{-2} - 4\right). \quad \text{(B.21)}$$

It is immediately apparent from eqs. (B.1)–(B.3), (B.6) that $\delta\bar{E}_a{}^i, \delta\bar{A}_b, \delta\bar{n}_{ab}$ and $\delta\bar{\Sigma}_{xy}$ decouple and evolve as follows:

$$\delta\bar{E}_a{}^i \propto e^{\left(1 - \mathcal{N}\left(1 - \bar{\Sigma}_{aa}\right)\right)t}, \quad \text{(B.22)}$$

$$\delta\bar{A}_b \propto e^{\left(1 - \mathcal{N}\left(1 - \bar{\Sigma}_{bb}\right)\right)t}, \quad \text{(B.23)}$$

$$\delta\bar{n}_{ab} \propto e^{\left(1 - \mathcal{N}\left(1 - \bar{\Sigma}_{aa} - \bar{\Sigma}_{bb}\right)\right)t}, \quad \text{(B.24)}$$

$$\delta\bar{\Sigma}_{xy} \propto e^{\left(1 - 3\mathcal{N}\right)t}. \quad \text{(B.25)}$$

Substituting eqs. (B.13), (B.17)–(B.18) for $\mathcal{N}, \bar{\Sigma}_{xx}$ and $\bar{\Sigma}_{yy}$, respectively, it is straightforward to verify that all the coefficients of t in the exponents are all positive, such that corresponding perturbations decay as $t \to -\infty$.

Similarly, the linearized equations (B.8)–(B.9) for $\delta\chi$ and $\delta\bar{W}_\chi$ form a closed system,

$$\partial_t \begin{pmatrix} \delta\chi \\ \delta\bar{W}_\chi \end{pmatrix} = \begin{pmatrix} 0 & (8/3)M^2/\sqrt{\kappa(\phi)} \\ -(8/3)M^2\bar{m}_\chi^2/\sqrt{\kappa(\phi)} & 1 - 8M^2 + M/m \end{pmatrix} \begin{pmatrix} \delta\chi \\ \delta\bar{W}_\chi \end{pmatrix}, \quad \text{(B.26)}$$

which is being continuously damped as $|t|$ grows since both eigenvalues

$$\lambda_\pm \approx \left(1 - 4M^2\right)\left(1 \pm \sqrt{1 - \frac{m_\chi^2 M^6 e^{2t}}{(1-4M^2)^3}}\right) \qquad (B.27)$$

corresponding to the coefficient matrix are both positive definite for $M \leq 0.2$. For example, for $M = 0.1, m_\chi = 300\Theta_0^{-1}$ and $t = -2$, $\lambda_+ \approx 1.9$ and $\lambda_- \approx 0.01$. Note that to evaluate $\kappa(\phi)$ at the Kasner-like stationary point, we used $\kappa(\phi) = (-\bar{V}/\bar{V}_0)^{M/m}$ and substituted $\bar{V}_0 = 0.1$ as defined in eq. (4.11).

The remaining four linearized variables $\delta\bar{\Sigma}_{xx}, \delta\bar{\Sigma}_{yy}, \delta\bar{W}_\phi$ and $\delta\bar{S}_\chi{}^x$ are determined by the closed system

$$\partial_t \delta\bar{\Sigma}_{xx} \approx \left(1 - 5M^2\right)\delta\bar{\Sigma}_{xx} + \frac{4}{3}\left(M^2 + 0.005\right)\delta\bar{\Sigma}_{yy} - 2M\delta\bar{W}_\phi + 2M\delta\bar{S}_\chi{}^x, \qquad (B.28)$$

$$\partial_t \delta\bar{\Sigma}_{yy} \approx -\frac{4}{3}\left(M^2 + 0.005\right)\delta\bar{\Sigma}_{xx} + \left(1 - 7M^2\right)\delta\bar{\Sigma}_{yy} + M\delta\bar{W}_\phi - M\delta\bar{S}_\chi{}^x, \qquad (B.29)$$

$$\partial_t \delta\bar{W}_\phi \approx \frac{2}{3}M(1 + 0.005M^{-2})(\delta\bar{\Sigma}_{xx} - \delta\bar{\Sigma}_{yy}) + \left(\frac{1}{2} - 8M^2\right)\delta\bar{W}_\phi + \frac{1}{2}\delta\bar{S}_\chi{}^x, \qquad (B.30)$$

$$\partial_t \delta\bar{S}_\chi{}^x \approx -M\left(4 + 0.01M^{-2}\right)\delta\bar{\Sigma}_{xx} + M(1 + 0.005M^{-2})\delta\bar{\Sigma}_{yy} + \frac{1}{2}\delta\bar{W}_\phi + \frac{1}{2}\delta\bar{S}_\chi{}^x. \qquad (B.31)$$

It is straightforward to verify using, e.g., a symbol mathematical computer program, that for $M \leq 0.2$, all four eigenvalues $\lambda_{1,2,3,4}$ of the coefficient matrix corresponding to the system of ordinary differential equations (B.28)–(B.31) have a positive real part. For example, for $M = 0.1$, $\lambda_1 \approx 0.94, \lambda_2 \approx 0.91, \lambda_3 \approx 0.80$, and $\lambda_4 \approx 0.13$. Since our time coordinate t is negative, running towards $-\infty$, a positive real part for all eigenvalues means all perturbations decay as $|t|$ grows and thus the Kasner-like stationary point solution with $\bar{S}_\chi{}^x \approx (3/4)M^{-1}$ is a stable attractor.

References

[1] PLANCK collaboration, *Planck 2018 results. VI. Cosmological parameters*, *Astron. Astrophys.* **641** (2020) A6 [*Erratum ibid.* **652** (2021) C4] [`arXiv:1807.06209`] [INSPIRE].

[2] J.M. Bardeen, P.J. Steinhardt and M.S. Turner, *Spontaneous Creation of Almost Scale-Free Density Perturbations in an Inflationary Universe*, *Phys. Rev. D* **28** (1983) 679 [INSPIRE].

[3] W.G. Cook, I.A. Glushchenko, A. Ijjas, F. Pretorius and P.J. Steinhardt, *Supersmoothing through Slow Contraction*, *Phys. Lett. B* **808** (2020) 135690 [`arXiv:2006.01172`] [INSPIRE].

[4] P. Creminelli, A. Nicolis and M. Zaldarriaga, *Perturbations in bouncing cosmologies: Dynamical attractor versus scale invariance*, *Phys. Rev. D* **71** (2005) 063505 [`hep-th/0411270`] [INSPIRE].

[5] D. Garfinkle, W.C. Lim, F. Pretorius and P.J. Steinhardt, *Evolution to a smooth universe in an ekpyrotic contracting phase with w > 1*, *Phys. Rev. D* **78** (2008) 083537 [`arXiv:0808.0542`] [INSPIRE].

[6] A. Ijjas, W.G. Cook, F. Pretorius, P.J. Steinhardt and E.Y. Davies, *Robustness of slow contraction to cosmic initial conditions*, *JCAP* **08** (2020) 030 [`arXiv:2006.04999`] [INSPIRE].

[7] A. Ijjas and R. Kolevatov, *Nearly scale-invariant curvature modes from entropy perturbations during the graceful exit phase*, *Phys. Rev. D* **103** (2021) L101302 [`arXiv:2102.03818`] [INSPIRE].

[8] A. Ijjas and R. Kolevatov, *Sourcing curvature modes with entropy perturbations in non-singular bouncing cosmologies*, *JCAP* **06** (2021) 012 [`arXiv:2012.08249`] [INSPIRE].

[9] A. Ijjas, F. Pretorius, P.J. Steinhardt and A.P. Sullivan, *The effects of multiple modes and reduced symmetry on the rapidity and robustness of slow contraction*, *Phys. Lett. B* **820** (2021) 136490 [`arXiv:2104.12293`] [ɪɴSPIRE].

[10] A. Ijjas and P.J. Steinhardt, *A new kind of cyclic universe*, *Phys. Lett. B* **795** (2019) 666 [`arXiv:1904.08022`] [ɪɴSPIRE].

[11] A. Ijjas, A.P. Sullivan, F. Pretorius, P.J. Steinhardt and W.G. Cook, *Ultralocality and slow contraction*, *JCAP* **06** (2021) 013 [`arXiv:2103.00584`] [ɪɴSPIRE].

[12] A.M. Levy, A. Ijjas and P.J. Steinhardt, *Scale-invariant perturbations in ekpyrotic cosmologies without fine-tuning of initial conditions*, *Phys. Rev. D* **92** (2015) 063524 [`arXiv:1506.01011`] [ɪɴSPIRE].

[13] M. Li, *Note on the production of scale-invariant entropy perturbation in the Ekpyrotic universe*, *Phys. Lett. B* **724** (2013) 192 [`arXiv:1306.0191`] [ɪɴSPIRE].

[14] V.F. Mukhanov, *Quantum Theory of Gauge Invariant Cosmological Perturbations*, *Sov. Phys. JETP* **67** (1988) 1297 [*Zh. Eksp. Teor. Fiz.* **94N7** (1988) 1] [ɪɴSPIRE].

[15] J.W. York Jr., *Gravitational degrees of freedom and the initial-value problem*, *Phys. Rev. Lett.* **26** (1971) 1656 [ɪɴSPIRE].